Manipulating bandwidth of light absorption at critical coupling: An example of graphene integrated with dielectric photonic structure

Jie Wang,[1,2] Ang Chen,[1,2] Yiwen Zhang,[1,2] Jianping Zeng,[1,2] Yafeng Zhang,[3] Xiaohan Liu,[1,2,*] Lei Shi,[1,2,*] and Jian Zi[1,2,*]

[1]*Department of Physics, Key Laboratory of Micro- and Nano-Photonic Structures (MOE), State Key Laboratory of Surface Physics, Fudan University, Shanghai 200433, China*

[2]*Collaborative Innovation Center of Advanced Microstructures, Fudan University, Shanghai 200433, China*

[3]*State Key Laboratory of Infrared Physics, Shanghai Institute of Technical Physics, Chinese Academy of Sciences, Shanghai 200083, China*

(Received 20 May 2019; revised manuscript received 11 July 2019; published 5 August 2019)

For an optical absorber, its efficiency and bandwidth determine ultimately its light-collection performance. A general way to realize the high-efficiency absorption and manipulate the absorption bandwidth is certainly important and highly desired. In this paper, based on the coupled-mode theory, a general strategy for tailoring the bandwidth of an absorber (to broaden or narrow it) is presented. A graphene-based absorber integrated with a lossless resonator is designed, and it is shown that by increasing the layer number of graphene and adjusting structure parameters, the broadband absorber at critical coupling could be realized. Meanwhile, by adjusting the location of graphene in the structure, an ultra-narrow-band absorber could also be realized. Present work of controlling both efficiency and bandwidth of an absorber would be particularly favorable for applications in light harvesting, light emitting devices, and optical modulators.

DOI: 10.1103/PhysRevB.100.075407

I. INTRODUCTION

The efficiency and bandwidth of an absorbing material play a vital role in practical applications, such as photothermal material [1–3] and a photovoltaic device [4–6]. Recently, critical coupling has attracted much interest because of the possibility to enhance the light absorption [7]. It is believed that the maximum and even perfect absorption could be realized if $\gamma_a = \gamma_r$, where γ_a is absorption rate of the absorbing material and γ_r is radiation rate of the photonic resonator. Various resonator structures, such as a photonic crystal (PhC) slab [8–11], metamaterial and metasurface [12,13], plasmonic structure [14–17], or dielectric waveguide [18–20] were designed and utilized. However, many works exploiting a single resonator to realize critical coupling, focused on the absorption efficiency and payed little attention to the bandwidth of the absorption. For broadband absorbers, the method of multimode resonators was preferentially employed [21,22]. To realize narrow-band absorption, the high-Q (quality factor) mode was often used [23,24]. These works concerned mainly the detailed structure parameters, obviously a simple and generic physical picture to manipulate the absorption bandwidth freely would be attractive.

In this paper, a general strategy for tailoring the bandwidth of an absorber with high efficiency is presented. Based on the coupled-mode theory (CMT) [25,26], a generic formula is derived to show that the absorption efficiency and especially the bandwidth of an absorber are mainly determined by the relationship between γ_a and γ_r of a resonator. For optimal absorption efficiency, i.e., critical coupling $\gamma_a = \gamma_r$ is satisfied, the larger (smaller) $\gamma_a + \gamma_r$ is, the wider (narrower) the absorption bandwidth will be and vice versa. From such analysis, both γ_r and γ_a need to be simultaneously adjusted over a wide range. To adjust γ_r, the lossless PhC slab is considered. It is shown that, by adjusting the structure parameters, such as the filling fraction and the slab thickness, γ_r can be varied as wide as two orders of magnitude. Meanwhile, it is also shown that γ_a can be adjusted by changing the amount of the absorbing material and its location in the resonance structure as wide as two orders of magnitude. Thus, the absorption bandwidth of an absorber can be tailored whereas the absorption efficiency could be maintained at a maximum value. Possibly, this paper presented would open up a new path to design the advanced photodetectors and modulators.

II. THEORETICAL ANALYSIS

Consider a single-mode optical resonator as shown in Fig. 1(a), whose optical behavior with amplitude a of the resonance mode coupled with m ports can be described by a CMT equation [25,26],

$$\frac{da}{dt} = -i\omega_0 a - \gamma_r a - \gamma_a a + \boldsymbol{D}^T \mathbf{S}_+, \tag{1}$$

$$\mathbf{S}_- = \boldsymbol{C}\mathbf{S}_+ + a\boldsymbol{D}. \tag{2}$$

where the vectors $\mathbf{S}_+ = (\mathbf{S}_{1+}, \mathbf{S}_{2+}, \ldots, \mathbf{S}_{m+})^T$, $\mathbf{S}_- = (\mathbf{S}_{1-}, \mathbf{S}_{2-}, \ldots, \mathbf{S}_{m-})^T$, and $\boldsymbol{D}$ are the amplitude of the flux of incoming and outgoing plane waves through each port and the coupling coefficient to all ports, respectively. The scattering matrix $\boldsymbol{C}$ describes the direct transmission between incoming and outgoing waves. As shown before, γ_r is the radiation coupling rate of the resonance mode, and γ_a is the intrinsic absorption rate of the system.

*Corresponding authors: liuxh@fudan.edu.cn; lshi@fudan.edu.cn; jzi@fudan.edu.cn

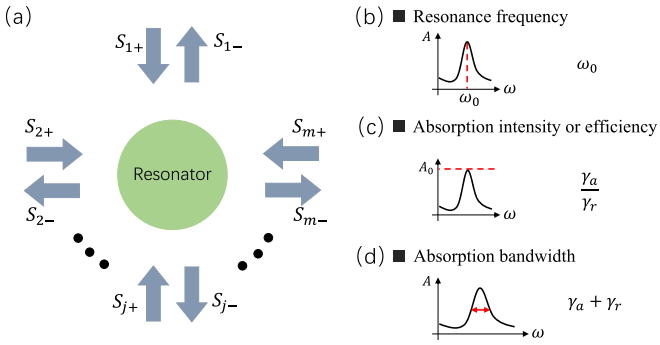

FIG. 1. (a) Schematic of an optical resonator system coupled with m free-space ports. The arrows indicate the incoming and outgoing waves. (b)–(d) Three key parameters describing absorption performance of a resonance absorber, (b) resonance frequency ω_0, (c) intensity, and (d) bandwidth of absorption. ω_0 is determined by the resonance mode the resonantor could support. The absorption intensity and bandwidth are determined by two rates, absorption rate γ_a and radiation rate γ_r. The ratio γ_a/γ_r and sum $\gamma_a + \gamma_r$ determine absorption intensity and bandwidth, respectively.

Suppose, for the resonance mode $a = a_0 e^{-i\omega t}$, Eq. (1) gives

$$a = \frac{\boldsymbol{D}^T \mathbf{S}_+}{-i(\omega - \omega_0) + (\gamma_r + \gamma_a)}. \tag{3}$$

Due to energy conservation and reciprocal theorem, $\boldsymbol{D}^+\boldsymbol{D} = 2\gamma_r$ and $\boldsymbol{C}\boldsymbol{D}^* = -\boldsymbol{D}$. Therefore, $\boldsymbol{D}^T = i(\sqrt{\gamma_1}, \sqrt{\gamma_2}, \ldots, \sqrt{\gamma_m})$ and $\sum_{j=1}^{m} \gamma_j = 2\gamma_r$, where γ_j is the coupling constant of port j. Light absorption of this system can be derived as

$$A = \frac{\mathbf{S}_+^* \mathbf{S}_+ - \mathbf{S}_-^* \mathbf{S}_-}{\mathbf{S}_+^* \mathbf{S}_+} = \frac{2\gamma_a a^* a}{\mathbf{S}_+^* \mathbf{S}_+}$$
$$= \frac{2\gamma_a \gamma_j}{(\omega - \omega_0)^2 + (\gamma_a + \gamma_s)^2}. \tag{4}$$

Assume the resonance mode coupled to each of the m ports with the same rate γ_j, $\gamma_j = 2\gamma_r/m$, and the absorption can be rewritten as

$$A = \frac{4}{m} \frac{\gamma_a \gamma_r}{(\omega - \omega_0)^2 + (\gamma_a + \gamma_r)^2}. \tag{5}$$

It is clear that the absorption peak of value A_0 occurs at the resonant frequency ω_0,

$$A_0 = \frac{4}{m} \frac{\gamma_a \gamma_r}{(\gamma_a + \gamma_s)^2} = \frac{4}{m} \frac{1}{\frac{\gamma_a}{\gamma_s} + \frac{\gamma_s}{\gamma_a} + 2}. \tag{6}$$

The absorption intensity or efficiency is determined by the ratio between γ_a and γ_r. When the absorption rate is equal to the radiation rate $\gamma_a = \gamma_r$, namely, critical coupling, the absorption reaches its maximum,

$$A_{\max} = \frac{1}{m}. \tag{7}$$

That is, the maximum absorption efficiency $A_{\max}$ of a single optical resonator is closely related to its port numbers. For a given resonator, the port number is known, and then, $A_{\max}$ can be determined.

Moreover, from Eq. (5), the absorption shows the symmetric Lorentzian line shape. The absorption bandwidth Γ^{FWHM} is defined as the full width at half maximum (FWHM). Suppose the half maximum absorption A_1 occurs at frequency ω_1, it has

$$A_1 = \frac{4}{m} \frac{\gamma_a \gamma_r}{(\omega_1 - \omega_0)^2 + (\gamma_a + \gamma_r)^2}. \tag{8}$$

From $\Gamma^{\mathrm{FWHM}} = 2(\omega_1 - \omega_0)$ and $A_0 = 2A_1$, the absorption bandwidth can be easily obtained as

$$\Gamma^{\mathrm{FWHM}} = 2(\gamma_a + \gamma_r). \tag{9}$$

From Eqs. (5), (6), and (9), it can be seen that the absorption performance of a system given is determined by three parameters ω_0, γ_a, and γ_r. The resonance frequency ω_0 determines the working frequency of a device and is determined by the resonance mode the system could support [Fig. 1(b)]. The absorption intensity represents the working efficiency of the system and is related to the ratio between γ_a and γ_r (γ_a/γ_r) [Fig. 1(c)]. At the resonance frequency, the intensity reaches its maximum value if the critical coupling condition $\gamma_a = \gamma_r$ is satisfied. The bandwidth is also an important parameter for a real device for optical signal processing and sensing applications. Equation (9) shows the absorption bandwidth is just twice the total damping rate $\gamma_a + \gamma_r$ [Fig. 1(d)]. This shows that adjusting the total rate can manipulate the absorption bandwidth. With simultaneous adjustment of γ_a and γ_r at critical coupling, controllable bandwidth of absorption can be realized. Therefore, it is realistic to manipulate the absorption bandwidth with high efficiency.

Next, as a model structure the absorbing material graphene integrated with lossless PhC slab is presented (another case that graphene-based absorber integrated with all-dielectric metamaterial is shown in the Supplemental Material [27], which includes Ref. [28].). This system has two ports ($m = 2$) and $A_{\max}$ is 50%. It will be shown how to change the structural parameters to adjust γ_r and γ_a and how to tailor the absorption bandwidth of an absorber.

III. REALIZATION OF A BROADBAND ABSORBER

γ_r of a resonator is one of the most important parameters, its range is directly related to the manipulation of the absorption bandwidth. γ_r is determined by the optical mode of a resonator and its structure parameters. In the present paper, the lossless PhC slab is adopted as the resonator. Due to the scattering of a periodic structure, guided modes in a high-refractive-index slab couple to the external radiation, forming leaky guided resonances [29]. Figure 2(a) shows a schematic of the investigated Si_3N_4 PhC slab. Simulation results are obtained by using two-dimensional rigorous coupled-wave analysis (diffract mode, RSOFT). The refractive index of Si_3N_4 is set as $n = 2$. Although the thickness h of the slab and the periodicity p of the structure are fixed as $h = 100$ and $p = 500$ nm, respectively, the filling fraction d/p is changed, where d is the diameter of the air hole. Figure 2(b) shows the simulated refection spectra at normal incidence as a function of wavelength and filling fraction represented by the diameter of the air hole. It can be seen that the bandwidth of the reflection spectra of all resonance modes first increases and then decreases with increasing filling fraction.

Here, only the lowest-order guided resonance among 600–700 nm wavelengths is considered. From both the

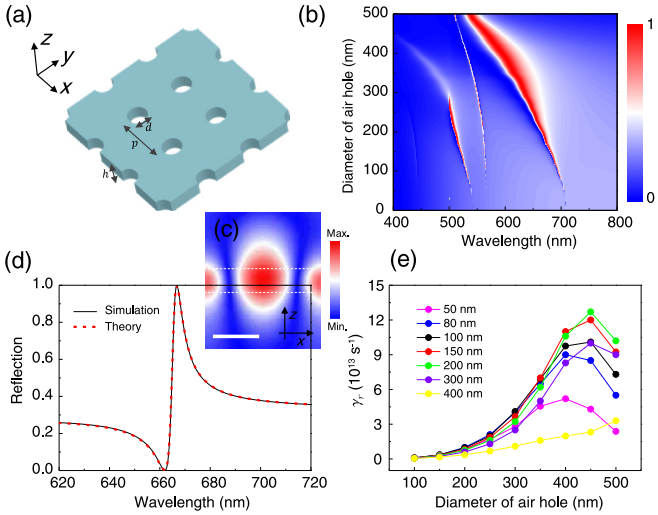

FIG. 2. (a) Schematic of a Si_3N_4 PhC slab which is a square lattice at each lattice point located one cylindrical air hole. (b) The reflection spectra as a function of wavelength and filling fraction represented by the diameter of the air hole at normal incidence. (c) shows the distribution of $|E|^2$ on the x-z cross-sectional plane through the center of air hole where the diameter of the air hole is $d = 200$ nm. The scale bar is 200 nm. (d) The reflection spectra of the PhC slab with $p = 500$, $h = 100$, and $d = 200$ nm. The CMT results (dashed red curve) agree excellently with the simulation (solid black curve). (e) γ_r of the resonance guided mode as a function of air hole diameter for different thicknesses of the slab.

electric-field distribution of the simulation [Fig. 2(c)] and the CMT, this lowest-order resonance mode is an even (TE-like) mode. γ_r can be obtained by fitting transmission and reflection spectra near a guided resonance with the CMT [30].

Figure 2(d) shows the reflection spectrum for $d = 200$ nm and $\gamma_r = 0.019 \times 10^{14}$ s^{-1}. It can be seen that the theory agrees excellently with the simulation result. As shown in Fig. 2(e), γ_r of the guided resonance exists as a maximum value. This phenomenon is understandable. For the ultrasmall filling fraction, i.e., for the short diameter of the air hole, the slab is more like a uniform Si_3N_4 film. The ability of the periodic structure to scatter guided resonance into the free space is weakened, resulting in a longer decay time for guided resonance and low γ_r. In the extreme case where the filling fraction is zero, the guided resonance is entirely trapped inside the slab, and γ_r would be 0. On the other hand, for the ultralarge filling fraction, i.e., for the big air holes, the slab seems like the air film. The low index-contrast slab could hardly support the guided mode, also resulting in a low γ_r. Thus, there must be a maximum γ_r within.

Other parameters, such as the thickness h, refractive index n of the slab, as well as different periodic structures are also considered to adjust γ_r. Here, the case with changing h is given. As shown in Fig. 2(d), for a fixed periodicity of $p = 500$ nm, the maximum γ_r can be further increased by one-third of the case of $d = 100$ nm by adjusting h. Therefore, in principle, by adjusting structure parameters or select other modes, γ_r could be adjusted over a wide range.

To realize broadband absorber with optimal efficiency, based on the above analysis, it needs to increase γ_a and satisfy the condition $\gamma_a = \gamma_r$. Increasing the amount of the absorbing material is an effective way to increasing γ_a, and in the present paper, it is performed by increasing layer numbers L of graphene. As shown schematically in the inset of Fig. 3(a), the graphene is intercalated at the center plane of the PhC slab. The graphene thickness and its optical constants are set as the same as Ref. [31]. From Figs. 3(a)–3(e), L is 1, 2, 4, 7, and 8, respectively. On one hand, the absorption efficiency of

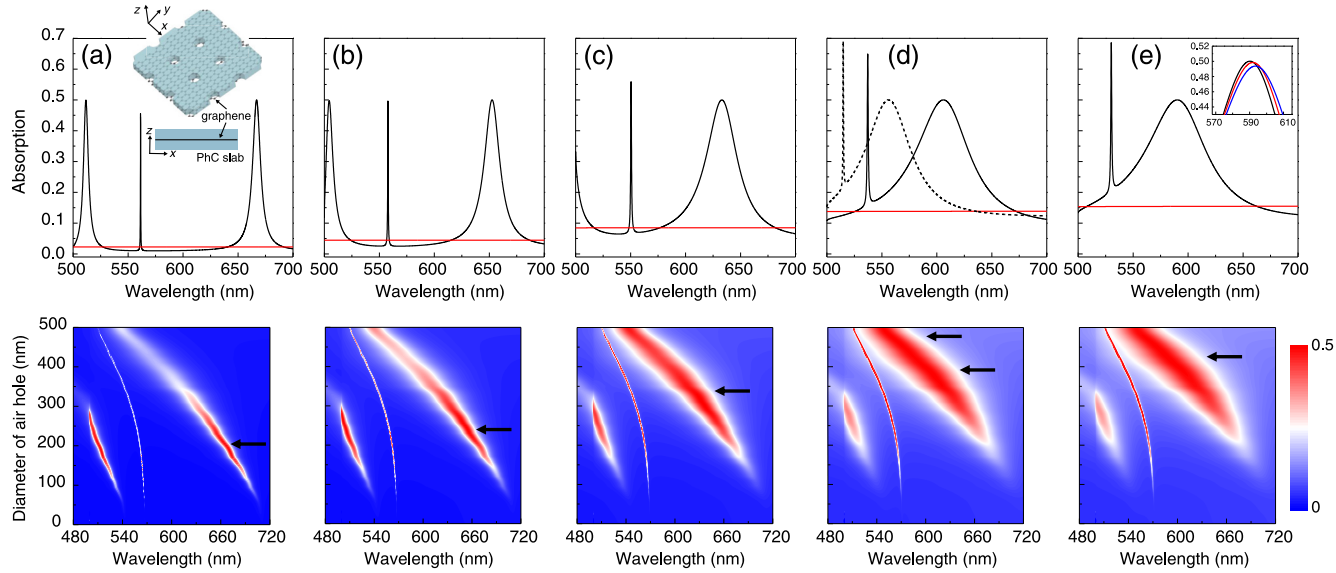

FIG. 3. (a)–(e) Upper black curves correspond to the graphene absorption for different layers at the critical coupling condition, and the lower panels show absorption spectra as a function of wavelength and filling fraction. Critical coupling points are marked by arrows. From (a)–(e), the layer numbers of graphene are increased as 1, 2, 4, 7, and 8, respectively. The red curves show the absorption of bare graphene with different layer numbers. The inset in (a): schematic of graphene located at the center plane of the slab. The inset in (e): detailed maximum absorption of graphene for eight (black curve), nine (red curve), and ten (blue curve) layers. For the PhC slab, $p = 500$ and $h = 100$ nm.

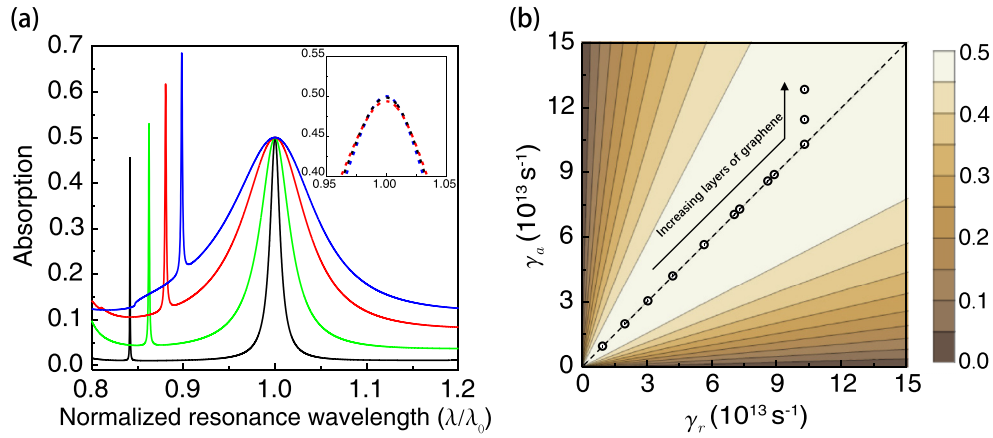

FIG. 4. (a) Absorption of graphene with different layers versus normalized resonance wavelength. Solid black, green, red, and blue curves represent the absorption of graphene with one, three, six, and eight layers, respectively, whereas dashed blue, black, and red curves in the inset (a) represent eight-, nine-, and ten-layer graphene, respectively. (b) Absorption efficiency of a two-port absorber at resonance wavelength as a function of absorption rate γ_a and radiation rate γ_r. Hollow dots represent γ_a and γ_r of the graphene-based absorber integrated with the PhC slab for different layers of graphene. The arrow shows the increasing trend of graphene layers. Parameters of the PhC slab are the same as those shown in Fig. 3.

bare graphene without the PhC slab is proportional to L (red curves), far below $A_{\max}$. Combined with the PhC slab results in a remarkable increase in the graphene absorption efficiency, even approaching $A_{\max}$, i.e., critical coupling. The critical coupling points (where the arrow marks in Fig. 3) for different L's can be easily found by changing the filling fraction. On the other hand, it can be found that the absorption bandwidth of graphene combined with the PhC slab continuously increases with L [panels (a)–(e)]. Specifically, the absorption bandwidth of monolayer graphene at critical coupling is only around 10 nm [Fig. 3(a)]. As shown in [Figs. 3(a)–3(e)], the absorption bandwidth at critical coupling is significantly increased with L. The maximum L of graphene that critical coupling still could be satisfied is 8 [Fig. 3(e)], and the absorption bandwidth is increased up to 11 times that of the monolayer graphene case. Further increasing graphene layers ($L > 8$), even though the absorption efficiency would drop down [the inset in Fig. 3(e)], the absorption bandwidth can be further increased. Additionally, in some cases, there will be two filling fractions satisfying the critical coupling condition. As seen in Fig. 3(d), it is at $d = 387.5$ nm (black solid curve) and 480 nm (black dashed curve) for seven-layer graphene, but the absorption bandwidth of the two is almost the same.

Figure 4(a) summarizes the results shown in Fig. 3 and shows the absorption at critical coupling as a function of normalized resonance wavelength. It can be found that, at critical coupling, the bandwidth of graphene can be sufficiently increased with layers. Figure 4(b) shows γ_a and γ_r as a function of L, which can be obtained by fitting absorption spectrum via the CMT. The arrow shows the trend of increasing layers of graphene. From one- to eight-layer graphene, both rates are manipulated along the line of the critical coupling and the direction of the increasing total damping rate $\gamma_a + \gamma_r$ [see Fig. 4(b)]. When increasing to nine-layer graphene $\gamma_a > \gamma_r$, the absorber evolves into the overcoupling regime, but $\gamma_a + \gamma_r$ is continuously increased. The absorption efficiency as a function of γ_a and γ_r is also shown on a contour. Even though γ_a and γ_r deviate from the critical coupling condition for

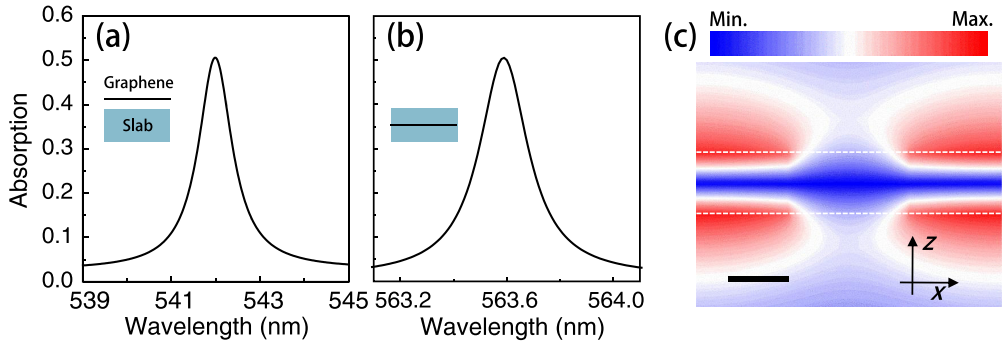

FIG. 5. (a) and (b) show the narrow-band and ultra-narrow-band absorptions of monolayer graphene at two different locations versus the wavelength for the odd mode, respectively. One is at 20 nm outside the boundary of the slab (a) whereas another is at the center plane of the slab (b). The insets in (a) and (b) are schematic cross-sectional views of the graphene-based absorber integrated with the PhC slab. (c) shows the distribution of $|E|^2$ at the resonance wavelength 561.66 nm on the x-z cross-sectional plane passing through the center of the air hole for $d = 200$ nm. The scale bar is 100 nm.

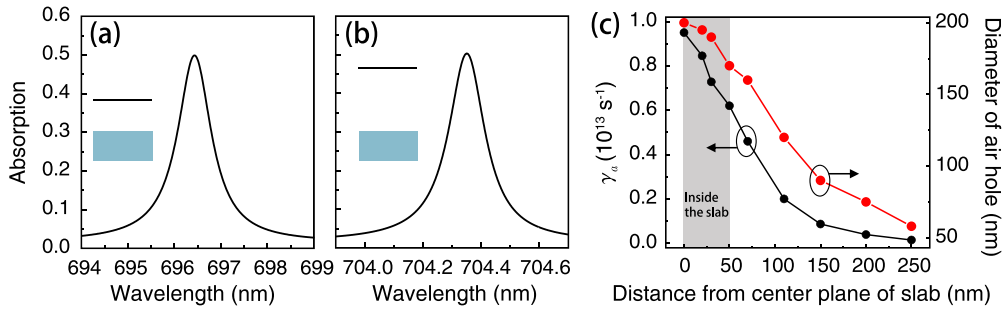

FIG. 6. (a) and (b) show the narrow-band and ultra-narrow-band absorptions of monolayer graphene located at 100 and 200 nm outside the boundary of the slab versus the wavelength for the even mode, respectively. The insets in (a) and (b) are schematic cross-sectional views of the graphene-based absorber integrated with the PhC slab. (c) γ_a and filling fraction of the PhC slab at critical coupling as a function of the distance of graphene away from the center plane of the slab.

$L > 8$, the absorption efficiency is still nearly 50% [inset in Fig. 4(a)]. This implies that there are wide ranges of tunability in optimized graphene-based optical absorbers, and the light harvesting materials with high performance could be realized.

IV. REALIZATION OF NARROW-BAND AND ULTRA-NARROW-BAND ABSORBERS

The discussion above is focused on how to broaden the bandwidth of an absorber with high efficiency. In fact, the narrow-band and ultra-narrow-band absorbers also have their valuable applications for selective band-stop filters [32] and active plasmonic switching [33]. In the following, a quite simple method to narrow down the bandwidth freely is proposed and even an ultra-narrow-band absorber could be realized. According to the theory presented above, in order to achieve narrow-band absorption, simultaneous reduction of $\gamma_a + \gamma_r$ is required under the condition of critical coupling. From the above results, the narrowest absorption bandwidth at critical coupling based on the TE-like mode is about 10 nm for monolayer graphene. To further decrease bandwidth, intuitionally thinking, the higher-Q mode with lower γ_r would be helpful. However, if γ_a remains unchanged, it would lead to the mismatch with γ_r and certainly depress the absorption performance. Interestingly, it is found that γ_a of the absorbing material is not only determined by its intrinsic absorption coefficient, but also closely related to the field distribution of the resonance mode and the location of the graphene in the resonator.

The narrow-band resonance guided mode around wavelength 500 nm as shown in Fig. 2(b) is first considered. Figure 5(c) shows the distribution of $|E|^2$ at the resonances on the x-z cross-sectional plane passing through the center of the air hole. The odd resonance (TM-like) in Fig. 5(c) has a nodal plane along the center plane of the PhC slab and stores more energy outside the slab. Figure 5 shows the critical coupling results of monolayer graphene located in two different locations. One is at 20 nm outside the boundary of the slab (area of higher-field intensity) [Fig. 5(a)] whereas another is at the center plane of the slab (area of lower-field intensity) [Fig. 5(b)]. Obviously, at critical coupling, the bandwidth of the latter is less than the former. This means far away from the high-field intensity area, less light coupled to the resonator could be absorbed by absorbing material, leading to effectively lower γ_a. As shown in Fig. 5(b), the narrow bandwidth could be reached as 0.2 nm.

The even resonance (TE-like) mode can also be used to realize the narrow-band absorber. Contrary to the distribution of the odd resonance mode, the even mode shown in Fig. 2(c) has an antinode, and more energy is stored inside the slab. According to the theory presented above, the farther away from the high-field intensity area, the lower γ_a and the narrower the bandwidth will be. In Fig. 6(a), compared to the result in Fig. 3(a), the bandwidth of graphene at 100 nm outside the boundary of the slab is only around 0.9 nm. Farther, as 200 nm away from the slab boundary where the electric field becomes weaker, the bandwidth could be further decreased to 0.14 nm. γ_a and the filling fraction of the PhC slab at critical coupling as a function of the distance of graphene away from the center plane of the slab are also plotted in Fig. 6(c). It should be noted that, because γ_r of the PhC slab could be as low as 0, the absorption bandwidth could be infinitely narrow. This corresponds to the location of the absorbing material in the ultra-weak-field area. Moreover, according to Kirchhoff's reciprocity, the structure's emissivity equates to its absorptivity, this method would also have possible potential applications in selective narrow-band emitters.

V. CONCLUSION

In conclusion, based on the CMT, the key parameters determining absorption performance of an optical absorber have been derived, especially for efficiency and bandwidth. For optimal absorption efficiency, i.e., under the condition of critical coupling $\gamma_a = \gamma_r$, the larger (smaller) $\gamma_a + \gamma_r$ is, the wider (narrower) the absorption bandwidth will be and vice versa. This generic theory can facilitate the design of tailoring the bandwidth of an absorber with high efficiency. Taking absorbing material graphene integrated with the lossless PhC slab as a model, manipulation of the broadband or narrow-band absorber at critical coupling has been demonstrated. By increasing the layer number of graphene and adjusting structure parameters, an optimal-efficiency absorber with 11 times bandwidth increase could be realized. Meanwhile, by adjusting the location of graphene in the structure, the ultra-narrow-band absorber at critical coupling has also been demonstrated. In principle, the absorption bandwidth could be nearly infinitely narrow. This paper would be valuable for

applications in light harvesting and emitting devices, optical modulators, filters, and so on.

ACKNOWLEDGMENTS

The authors thank Y. Xia for helpful discussions. The work was supported by the 973 Program and the China National Key Basic Research Program (Programs No. 2015CB659400, No. 2016YFA0301100, No. 2016YFA0302000, and No. 2018YFA0306201) and the National Science Foundation of China (Grants No. 11774063, No. 11727811, No. 91750102, and No. 11604355). The research of L.S. was further supported by the Science and Technology Commission of Shanghai Municipality (Grants No. 17ZR1442300 and No. 17142200100).

[1] O. Neumann, C. Feronti, A. D. Neumann, A. J. Dong, K. Schell, B. Lu, E. Kim, M. Quinn, S. Thompson, N. Grady, P. Norderlander, M. Oden, and N. J. Halas, Proc. Natl. Acad. Sci. USA **110**, 11677 (2013).

[2] Z. Y. Fang, Y. R. Zhen, O. Neumann, A. Polman, F. J. García de Abajo, P. Nordlander, and N. J. Halas, Nano Lett. **13**, 1736 (2013).

[3] X. L. Zhu, C. Vannahme, E. Højlund-Nielsen, N. A. Mortensen, and A. Kristensen, Nat. Nanotechnol. **11**, 325 (2016).

[4] M. W. Knight, H. Sobhani, P. Nordlander, and N. J. Halas, Science **332**, 702 (2011).

[5] M. L. Brongersma, P. Nordlander, and N. J. Halas, Nat. Nanotechnol. **10**, 25 (2015).

[6] K. F. Mak and J. Shan, Nat. Photonics **10**, 216 (2016).

[7] A. Yariv, Electron. Lett. **36**, 321 (2000).

[8] J. R. Piper and S. H. Fan, ACS Photon. **1**, 347 (2014).

[9] J. R. Piper, V. Liu, and S. H. Fan, Appl. Phys. Lett. **104**, 251110 (2014).

[10] Y. H. Liu, A. Chadha, D. Y. Zhao, J. R. Piper, Y. C. Jia, Y. C. Shuai, L. Menon, H. J. Yang, Z. Q. Ma, S. H. Fan, F. N. Xia, and W. D. Zhou, Appl. Phys. Lett. **105**, 181105 (2014).

[11] C. C. Guo, Z. H. Zhu, X. D. Yuan, W. M. Ye, K. Liu, J. F. Zhang, W. Xu, and S. Q. Qin, Adv. Opt. Mater. **4**, 1955 (2016).

[12] S. A. Tretyakov and S. I. Maslovski, Microwave Opt. Technol. Lett. **38**, 175 (2003).

[13] C. A. Valagiannopoulos, J. Vehmas, C. R. Simovski, S. A. Tretyakov, and S. I. Maslovski, Phys. Rev. B **92**, 245402 (2015).

[14] M. Zhou, L. Shi, J. Zi, and Z. F. Yu, Phys. Rev. Lett. **115**, 023903 (2015).

[15] J. Wang, D. Z. Han, A. Chen, Y. Y. Dai, M. Zhou, X. H. Hu, Z. F. Yu, X. H. Liu, L. Shi, and J. Zi, Phys. Rev. B **96**, 195419 (2017).

[16] S. Kim, M. S. Jang, V. W. Brar, K. W. Mauser, L. Kim, and H. A. Atwater, Nano Lett. **18**, 971 (2018).

[17] A. Sheverdin and C. Valagiannopoulos, Phys. Rev. B **99**, 075305 (2019).

[18] H. Zhao, W. S. Fegadolli, J. K. Yu, Z. F. Zhang, L. Ge, A. Scherer, and L. Feng, Phys. Rev. Lett. **117**, 193901 (2016).

[19] S. Suwunnarat, D. Halpern, H. Li, B. Shapiro, and T. Kottos, Phys. Rev. A **99**, 013834 (2019).

[20] W. R. Sweeney, C. W. Hsu, S. Rotter, and A. D. Stone, Phys. Rev. Lett. **122**, 093901 (2019).

[21] Y. X. Cui, J. Xu, K. H. Fung, Y. Jin, A. Kumar, S. L. He, and N. X. Fang, Appl. Phys. Lett. **99**, 253101 (2011).

[22] K. Aydin, V. E. Ferry, R. M. Briggs, and H. A. Atwater, Nat. Commun. **2**, 517 (2011).

[23] L. J. Meng, D. Zhao, Z. C. Ruan, Q. Li, Y. Q. Yang, and M. Qiu, Opt. Lett. **39**, 1137 (2014).

[24] A. S. Feng, Z. J. Yu, and X. K. Sun, Opt. Express **26**, 28197 (2018).

[25] H. A. Haus, *Waves and Fields in Optoelectronics* (Prentice Hall, Englewood Cliffs, NJ, 1984).

[26] S. H. Fan, W. Suh, and J. D. Joannopoulos, J. Opt. Soc. Am. A **20**, 569 (2003).

[27] See Supplemental Material at https://link.aps.org/supplemental/10.1103/PhysRevB.100.075407 for the case of the graphene-based absorber integrated with all-dielectric metamaterial.

[28] F. H. L. Koppens, D. E. Chang, and F. J. García de Abajo, Nano Lett. **11**, 3370 (2011).

[29] S. H. Fan and J. D. Joannopoulos, Phys. Rev. B **65**, 235112 (2002).

[30] C. W. Hsu, B. Zhen, J. Lee, S. Chua, S. G. Johnson, J. D. Joannopoulos, and M. Soljačić, Nature (London) **499**, 188 (2013).

[31] M. Bruna and S. Borini, Appl. Phys. Lett. **94**, 031901 (2009).

[32] X. J. Wang, H. Y. Meng, S. Liu, S. Y. Deng, T. Jiao, Z. C. Wei, F. Q. Wang, C. H. Tan, and X. G. Huang, Mater. Res. Express **5**, 045804 (2018).

[33] H. S. Chu and C. H. Gan, Appl. Phys. Lett. **102**, 231107 (2013).